Multiple Strip Photo Mixing Demodulator for 3D Imaging Implemented on High Resistivity Silicon

Quazi Delwar Hossain[1*], Gian-Franco Dalla Betta[2], Lucio Pancheri[3], David Stoppa[3], Sagar Kumar Dhar [4]
[1]Department of EEE, Chittagong University of Engineering and Technology (CUET),
Chittagong-4349, Bangladesh
[2]Department of Information Engineering and Science, University of Trento,
38123 Trento, Italy
[3]Fondazione Bruno Kessler (FBK),
38123 Trento, Italy
[4]Department of Electrical and Electronic Engineering, Premier University,
Chittagong, Bangladesh
*quazi@cuet.ac.bd

Abstract—**In this paper a multiple strip photo mixing demodulator fabricated on high resistivity silicon is described. The performance such as DC characteristics, demodulation contrast and non-linearity problem of a test sample are simulated and experimentally estimated. The experimental results exhibit a good DC charge separation and good dynamic demodulation capabilities up to 30MHz. The influence of modulation frequency and voltage on this device is also discussed. This test device corresponds to the first step towards incorporating a high resolution Time of Flight (TOF) based 3D image sensor.**

Index Terms—**Time of flight; 3D imaging; Photo mixing demodulator**

I. INTRODUCTION

3D vision system is a versatile and commercially important technology. Lot of efforts have been concentrated to develop a standard 3D imager. Range-imaging sensors accumulate large amount of three-dimensional (3D) data from visible surfaces in a scene and can be used in a large growing applications such as indoor surveillance purpose, pedestrian safety, robotics, bio medical applications etc. 3D image is concerned with extracting information from the geometric evaluation of three co-ordinates and the texture of the visible surfaces in a scene.

Several types of optical techniques for 3D imaging range measurement are available in the literature among which the most important one is time-of-flight (TOF) principle that is intensively investigated. The third dimension, i.e. depth information, can be determined by correlating the reflected modulated light signal from the scene with a reference signal synchronous with the light source modulation signal [1]. The state of the art of TOF based 3D imagers so far reported and can be divided in different categories, differing for the type of photodetector use in the pixels. A standard photodiode coupled with complex readout circuitry is proposed and the indirect time-of-flight is used [2-5]. This approach can yield an accuracy of a few cm over a maximum range of a few meters. The photo demodulator is implemented with different types of special technologies such as: CMOS/CCD, CCD and non-standard CMOS or hybrid approach. In this demodulator the photo generated charge is 'mixed' on two or more photo-gates thus achieving an intrinsic demodulation effect [6-9]. A range of powerful contributions to dynamic 3D-vision, the Photonic Mixer Device (PMD) is an interesting solution that is reported in [10]. A major performance improvement has been reported in [11]. The role of detection and demodulation in a single device use a modulated electric field that penetrates deeper into the substrate, thus enhancing the charge separation and collection mechanism.

In this work, we present a multiple strip field assisted photo mixing demodulator fabricated in custom technology. The device architecture with its working principle and ISE-TCAD simulation are introduced in section II. In section III, the device electro-optical characterization is reported. Finally the paper is concluded in section IV.

II. DEVICE DESIGN AND WORKING PRINCIPLE

This device consists of fingered type electrodes i.e. multi tap CAPD device. Fig. 1 (a) and (b) shows the cross sectional view and the layout of the device respectively. It consists of nine detection electrodes. Among these detection electrodes, the seven central regions (as shown in Fig. 1 from region 2 to region 8) consist of a detection junction (p+ region) and two substrate contacts (n+ region). The rest of detection regions contain one detection junction and one substrate contact, like the region 1 and 9 shown in Fig. 1. Finally this device has four electrodes, two collecting electrodes (V_{d1} and V_{d2}) that are connected to the detection junction and two modulating electrodes (V_{m1} and V_{m2}) that are connected to the device substrate.

This device is also surrounded with an n+ bulk-contact, shared along the array and placed at a minimum distance of about 20μm from the pixel boundary. A p+ ring is placed surround the n+ bulk-contact maintaining the distance of about 20μm for better isolation. The total area of this device

978-1-4673-1436-7/12/$31.00 ©2012 IEEE

is 400µm × 400 µm. The distance between the adjacent modulating electrodes is 20 µm.

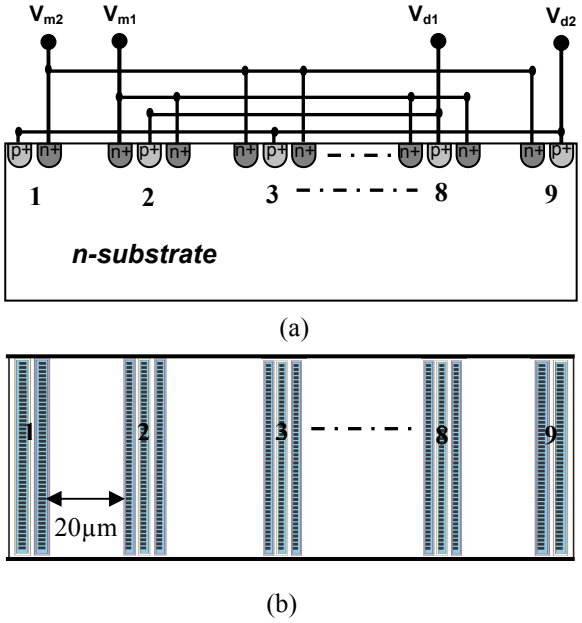

Fig. 1 (a) Cross sectional view of multiple strip CAPD and (b) Device layout

In this device an effective potential gradient is applied to the multiple modulating electrodes that speed up the signal charges transferring to the detection regions.

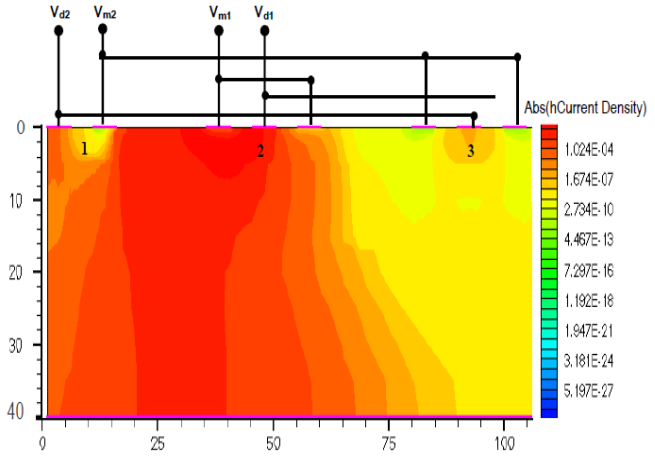

Fig. 2 Simulated hole current density under illumination

The potential difference $\Delta V = V_{m2} \sim V_{m1}$ defines at which region the hole current is detected i.e. detecting electrodes V_{d1} or V_{d2}. The operational behaviour of the multi tap device is investigated using the device simulation software ISE-TCAD. Fig. 2 shows the hole current density of this device with a voltage difference applied between two modulating electrodes (where $V_{m1} > V_{m2}$) and a 780 nm light incident on the device surface. Most of the generated holes move toward the collecting electrode V_{d1}, guided by the electric field. In this simulation picture, it shows the region 1, 2 and 3 according to the cross sectional view of the device shown in Fig. 1(a).

III. Device Test and Performance Characteristics

After the customize fabrication of the test device at Fondazione Brouno Kessler (**FBK**), Trento, Italy, the dc and ac characterization is carried out.

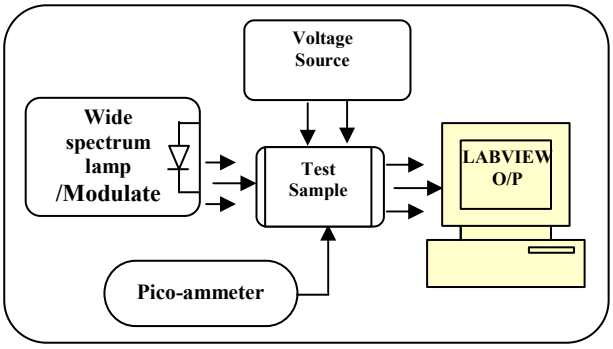

Fig. 3 Experimental setup for DC characterizations

Fig. 3 shows the set up for the measurement of DC characterization of the test device. The device is illuminated with a wide spectrum lamp. In this measurement the required voltage at different electrodes can be supplied with a voltage source. A Pico ammeter is used to read out the detection current.

Fig. 4 shows the DC characteristics of the device under the illumination of wide spectrum light, it illustrates a good DC charge separation efficiency. Thus indicating the device is potentially enabling a very efficient mixing process from low guiding modulation voltages.

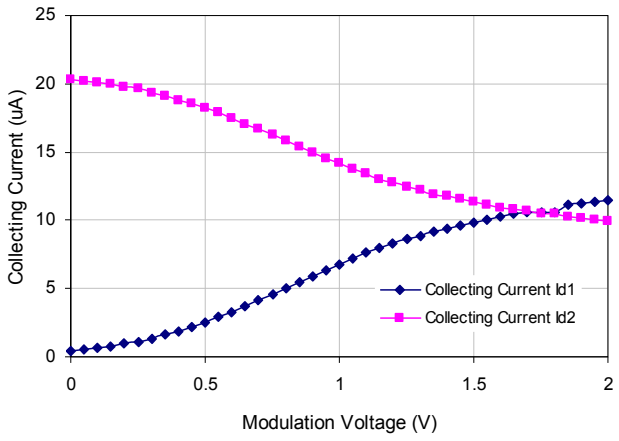

Fig. 4 DC characteristics of the device under the illumination of wide spectrum light.

The modulating voltage ΔV allows demodulation of the photonic signal. If $V_{m2} > V_{m1}$ the hole current is detected in V_{d2} region, for $V_{m1} > V_{m2}$ it moves to the opposite detection region. As the collecting electrodes for V_{d1} and V_{d2} are not equal, the DC characteristics of this device are not symmetrical as linear-shaped device.

The average current measurement at the collecting electrodes and the dynamic demodulation contrast is characterized for the test device using the set up is shown in Fig. 5.

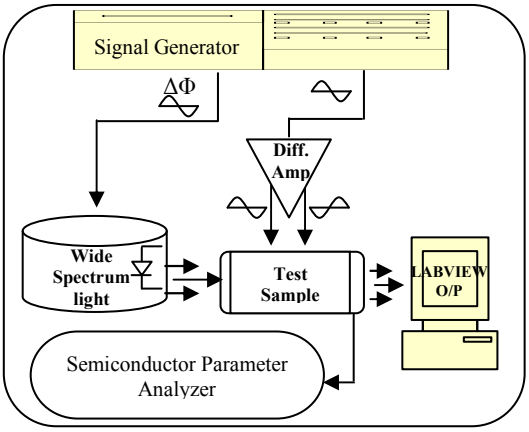

Fig. 5 Experimental setup for Dynamic characterizations

A signal generator is used to generate two sine wave signals. One of the two signals is used to modulate a laser emitter and the other is connected to the input of a differential amplifier. The amplifier outputs with 180^0 phase shift are connected to the modulating of electrodes V_{m1} and V_{m2} of the device. The detection current through the collecting electrodes V_{d1} and V_{d2} are read out with a Semiconductor Parameter Analyzer. For this measurement, three sine wave signals are used with an appropriate synchronization. Finally, a software program for the interface with PC and the data acquisition is developed with LABVIEW. The average current is measured under a 650nm red laser with 90% modulation depth used to illuminate the test device at different modulation frequencies.

The sensor ability to separate and transfer the charges to the corresponding output node can be expressed as a demodulation contrast. It is obvious that the demodulation contrast depends on the amplitudes of the modulation voltages.

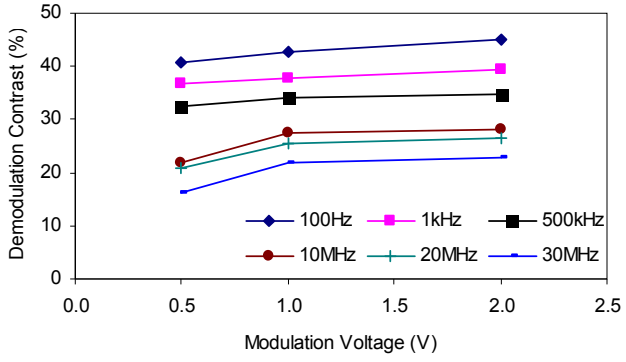

Fig. 6 Demodulation contrast at different modulation voltage

Fig. 6 shows the growth of demodulation contrast for the device as a function of the modulation voltage amplitude at different frequencies. Increasing the modulation voltage basically increases the majority current that cause the drift of the minority carriers, namely electrons. As the modulation voltage is applied to the modulating electrodes, the photo generated electrons arrive at the detector node of the device. If applying the larger voltages the electrical field extend deeper in the substrate so that more electrons reach detection node resulting in a higher demodulation contrast. However, at the same time the power consumption is increased. So the value of the modulation voltage amplitude should be carefully chosen.

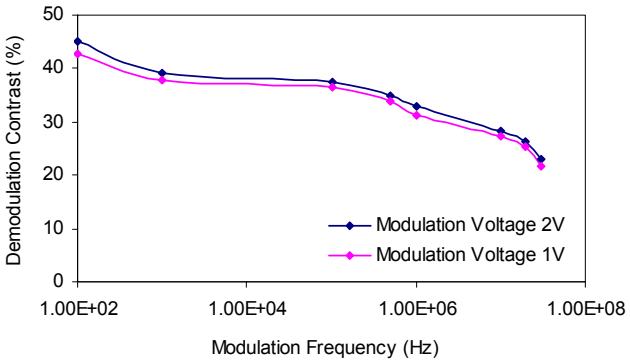

Fig. 7 Demodulation contrast at different modulation voltage

Fig. 7 shows the demodulation contrast at different modulation frequencies. The decrease of the demodulation contrast with frequency can be described with respect to time lagging. The photoelectrons generated more deeply in the epitaxial layer need more time to reach the active region where the demodulating electric field is present and thus reduces the demodulation contrast.

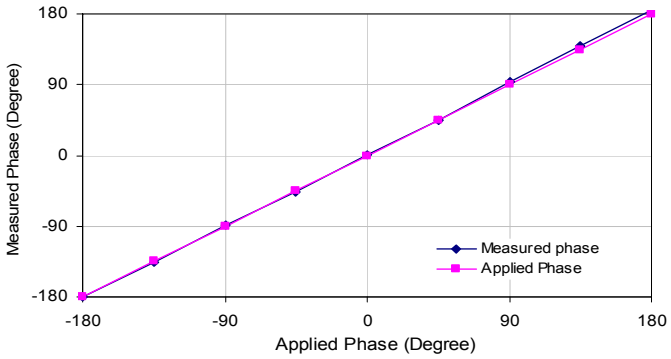

Fig. 8 Phase linearity measurement for Multiple Strip CAPD.

A set of phase measurements are performed on the device. In these measurements a variable phase delay $\Delta\varphi$ is applied between two modulating electrodes and the laser input to illuminate the device. The value $\Delta\varphi$ of can be recovered acquiring four amplitude measurements with four different phase shifts θ_1, θ_2, θ_3 and θ_4 applied to the modulated laser signal considered as -180°, -90°, 0° and +90° respectively [12]. It can be represented by the equation (i) given below:

$$\Delta\varphi = \arctan\frac{I(\theta_1) - I(\theta_3)}{I(\theta_2) - I(\theta_4)} \quad \ldots\ldots\ldots \text{(i)}$$

The measurement is performed considering sinusoidal wave modulation signals at 20 MHz, and the resulting phase is

reported in Fig. 8 for multiple strips device. The maximum linearity error of multi strip CAPD device is 3.9 % for sinusoidal wave modulation, thus, confirming the good linearity of the device.

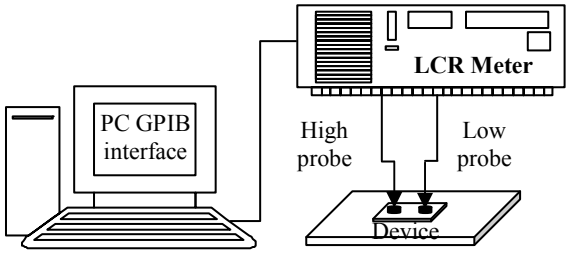

Fig. 9 Experimental set-up for capacitance measurement

The experimental set-up for capacitance measurement of the CAPD is shown in Fig. 9. An LCR Meter is used for accurate measurement of capacitance. In this experiment the LCR meter serves two main functions. They are to measure the capacitance of the device and to supply the required voltage bias across the junction. The LCR meter and the experiment are controlled using a LABVIEW program via GPIB interface between the Computer and the LCR meter.

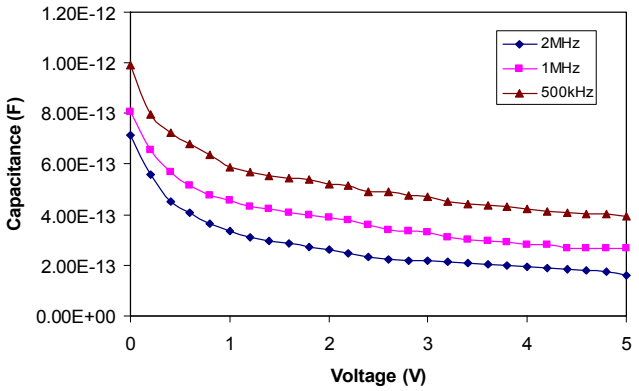

Fig. 10 C-V characteristics

Fig. 10 shows C-V response under different frequencies of the device. It shows that a higher reverse bias produces a lower capacitance due to a larger depletion width. For higher reverse bias, more electrons are attracted to the n-side, holes attracted to the p-side. This result increases the depletion region. In this figure it shows that, at lower frequency the capacitance is larger than at higher frequency. Due to the deep-level impurities in the space charge region make the capacitance to be frequency dependent because of their finite charging and discharging time [13], [14].

III. Conclusion

This paper has covered the most relevant issues related to the characterization of Photo Mixing Demodulator fabricated in a custom technology on high resistivity silicon substrates. A 400µm × 400µm structure with multiple strips have been considered and tested in terms of electrical and electro-optical performance. In particular, we have investigated the DC and dynamic demodulation performance of a multiple strip device. In the multiple strip CAPD devices, the effective potential gradient is applied to the multiple modulating electrodes, a fact that speeds up the signal charges transferring to the detection regions. The measured dynamic demodulation contrast is more than 20% at 30 MHz modulation frequency. The maximum phase linearity error between the applied phase and the measured phase is 3.9%. However, as multiple strip conductors are used in this device, the fill factor is very low with respect to the device size.

Acknowledgement

This research work is partially supported by the Fondazione Bruno Kessler (FBK), Trento, Italy in chip fabrication and device measurement.

IV. References

[1]. I.Moring, T.Heikkinem, R.Myllyla and A.Kilpela, “Acquisition of three dimensional image data by a scanning laser range finder” Opt.Eng. Vol28 pp 897-905,1989.

[2]. R.Jeremias, W.Brockherde, G.Doemens, B.Hosticka, L.List and P.Mengel, “ A CMOS Photosensor Array for 3D Imaging Using Pulsed Laser” , Proceedings of ISSCC’01,paper 16.5,Sanfransisco (CA) USA,Feb, 2001.

[3]. O .M. Schrey, 0. Elkhalili, P. Mengel', M. Petermann, W. Brockherde, B.J. Hosticka “A 4x64 Pixel CMOS Image Sensor for 3D Measurement Applications” , IEEE Journal of Solid State Circuits, vol.39, no.7, pp.1208-1212,July, 2004.

[4]. David Stoppa, Luigi Viarani, Andrea Simoni, Lorenzo Gonzo, Mattia Malfatti, Gianmaria Pedretti, “A 16x16-Pixel Range-Finding CMOS Image Sensor” Proceedings of IEEE European Solid-State Circuits Conference- ESSCIRC’04, pp. 419-422, September, 2004.

[5]. D.Stoppa, L.Viarani ,A.Simoni, L.Gonzo,M.Malfatti, G.Pedretti “ A 50×30 pixel CMOS sensor for TOF-based real time 3D imaging” proceedings of the IEEE workshop on CCD and advanced Image sensors, pp.230-233,2005.

[6]. R.lange and P. Seitz, “Solid- State Time-of-Flight Camera”, IEEE Journal of Quantum Electronics, Vol.37,no.3, pp. 390-397, March 2001.

[7]. R. Miyagawa and T. Kanade, “CCD-Based Range-Finding Sensor”, IEEE Trans. ED, vol.44, no.10, pp.1648-1652, 1997.

[8]. T. Oggier, M. Lehmann, R.Kaufmann, M. Schweizer, M. Richter, P. Metzler, G.Lang, F. Lustenberger, N. Blanc,“An all solid-state optical range camera for 3D real-time imaging with sub-centimeter depth-resolution(SwissRanger), Proceeding of SPIE Vol.5249, pp. 634-645, 2003.

[9]. Mesa Imaging website: http: www.swissranger.ch

[10]. Rudolf Schwarte, “Dynamic 3D Vision”, Proceedings of International Symposium on Electron Devices for Microwave and Optoelectronic Applications, pp.241-248, 15-16 November, 2001.

[11]. Van Nieuwenhove, W.VanDer Tempel and M.Kuijik, “Novel Standard Detector using majority for guiding Photo-Generated Electrons towards Detecting Junctions”, Proceedings Symposium IEEE/LEOS Benelux Chapter, pp.229-232, 2005.

[12]. R. Lange, P. Seitz, A. Biber and R. Schwarte. “Time-of Flight Range Imaging with a Custom Solid State Image Sensor”, *EOS/SPIE International Symposium*. Munich, Germany, June 14-18 1999, pp. 180-191.

[13]. D. K. Schroder, *Semiconductor material and device characterization*, 2nd ed. New York: Wiley, 1998.

[14]. C. F. Robinson, "Micro probe analysis," 1973.